

3-2 Ionospheric Irregularities and the SEALION Project

3-2-1 Outline of the SEALION Project and Initial Results

MARUYAMA Takashi, SAITO Susumu, KAWAMURA Masabumi, NOZAKI Kenro, UEMOTO Jyunpei, TSUGAWA Takuya, JIN Hidekatsu, ISHII Mamoru, and KUBOTA Minoru

An ionosonde network including a meridional chain and east-west pairs was established in the Southeast Asian area. Three of five ionosondes are along the magnetic meridian of 100° E; two are close to the magnetic conjugate points in Northern Thailand and West Sumatra, Indonesia, and the other is near the magnetic equator in the Malay Peninsula, Thailand. The fourth and fifth ionosondes are also near the magnetic equator and low latitude in Vietnam but separated by about 6.3° towards east from the meridional chain. For a preliminary data analysis, nighttime ionospheric height variations at the three stations of the meridional chain were examined. The results demonstrate that the coordination of the network has a great potential for studying ionosphere/thermosphere dynamics. Through the assistance of model calculations, thermospheric neutral winds were inferred and compared with the HWM93 empirical thermospheric wind model. Higher-order wind variations that are not represented in the empirical model were found.

Keywords

Plasma bubble, Thermospheric dynamics, Transequatorial wind, Convergence wind, $\mathbf{E} \times \mathbf{B}$ drift

1 Introduction

The two most fundamental parameters that describe the status of the ionosphere are the maximum electron density (N_mF_2) and the height at which electron density reaches its maximum (h_mF_2). The fact that the ionospheric electron density reaches its maximum at a given height was first described by Chapman [1]. He conceived an idealized atmosphere in which the atmospheric density decreases exponentially with height. The scale height of atmospheric density determines h_mF_2 through a transition from a chemical equilibrium at lower altitudes to a diffusive equilibrium

at higher altitudes [2][3]. The actual ionosphere is not that static and simple. In a mid-latitude region, the ionospheric height is varied significantly by the $\mathbf{E} \times \mathbf{B}$ drift of plasma caused by the effects of an eastward electric field and a geomagnetic field, or by plasma moving along the magnetic field lines through collisions between neutral atmospheric particles and ions. Changes in h_mF_2 and N_mF_2 are closely related. As the ionospheric height rises, the electron density increases due to the smaller recombination rate at higher altitudes [4][5]. Variations in N_mF_2 in a low-latitude region are even more complex than in a mid-latitude region. On the magnetic equator,

the $\mathbf{E} \times \mathbf{B}$ drift caused by an eastward electric field will lift the ionospheric height, thereby reducing the collision frequency between ions and neutral atmospheric particles at higher altitudes, causing the plasma to be diffused toward a low latitude region along the magnetic field line under the influence of gravitational force. As a result, $N_m F_2$ on the magnetic equator decreases [6][7]. This phenomenon is called the “fountain effect.” Diffusion toward a low latitude region induces increases in $N_m F_2$ centered at a given latitude in the northern and southern hemispheres. The appearance of two peaks across the magnetic equator is called an “equatorial anomaly” [8][9]. Neutral winds traversing the magnetic equator or transequatorial winds also add to the complexity of electron density distributions around the magnetic equator. As plasma moves along the magnetic field lines dragged by neutral winds, it reduces the electron density upwind of the magnetic equator and increases it downwind at low latitudes. As in a mid-latitude region, the ionospheric height is raised by the equatorward wind and lowered by the poleward wind. Consequently, a smaller recombination rate caused by rising ionospheric heights results in higher electron density upwind and reductions downwind. The relative significance between both competing effects determines the actual variations in electron density. Sharma and Hewens [10] suggested that the crest density in the equatorial anomaly is higher in the winter hemisphere than in the summer hemisphere as a result of transequatorial winds carrying plasma from the summer hemisphere to the winter hemisphere. A similar picture of north-south asymmetry can be found in Fig. 9b of Maruyama and Matuura [11]. In this diagram, $N_m F_2$ is found higher in the northern (winter) hemisphere despite its low $h_m F_2$. Walker and Chan [12] demonstrated through model calculations of $N_m F_2$ and $h_m F_2$ that the complex observed facts described above represent the result of transequatorial wind.

When compared with $N_m F_2$ that varies in a complex manner under the influence of external forces, $h_m F_2$ responds to external forces far

more directly. The movement of plasma perpendicular to the magnetic field lines driven by an east-west electric field ($\mathbf{E} \times \mathbf{B}$ drift) and that of plasma in the direction of magnetic field lines dragged by neutral winds will be manifested more directly in ionospheric height variations [3][13][14].

One key role of variations in ionospheric height in a low-latitude region is related to ionospheric plasma instability. The lower part of the ionosphere extinguishes rapidly after sunset. Then, the electron density gradient steepens in the vertical direction, with the result of Rayleigh-Taylor (R-T) instability making plasma bubbles easier to form. R-T instability grows at higher rates at higher ionospheric heights where the collision frequency between ions and neutral atmospheric particles diminishes; the upward $\mathbf{E} \times \mathbf{B}$ drift caused by an enhanced eastward electric field (prereversal enhancement) right after sunset plays a significant part in lifting the ionospheric height. This enhanced eastward electric field is caused by the dynamo effect resulting from neutral wind at the ionospheric F-region height [15]–[18]. Even a strong transequatorial wind exceeding $\sim 100 \text{ ms}^{-1}$ would induce an apparent rise in equatorial ionospheric height (particularly in the bottomside ionosphere). This is an effect of blowing-off plasma in a relatively short magnetic flux tube passing through the bottomside ionosphere near the magnetic equator, but differs from the electric field effect in that it does not induce plasma instability [19]. The suppression of R-T instability by transequatorial neutral winds is the possible effect of sharply increasing Pedersen conductivity due to plasma being depressed downwind along the magnetic field lines [11][20]–[22]. That is, perturbation electric fields generated near the magnetic equator in conjunction with R-T instability are short-circuited in a low-latitude region by way of highly conductive magnetic field lines, resulting in suppressed instability.

Variations in ionospheric height were mentioned as being more direct than those in maximum electron density as responses to external

forces, but variations caused by a zonal electric field and those caused by winds in the magnetic meridional plane have a very different significance in R-T instability and must be distinguished. Yet, the task of distinguishing between the effects of electric fields and winds with data from a limited number of available observation points is not necessarily easy.

Many attempts have been made to derive neutral winds from changes in $h_m F_2$ in a mid-latitude region [13][23]–[27]. Among those attempts, Miller et al. [24] determined a numeric coefficient for linking the horizontal component of neutral wind in the magnetic meridional plane and deviations in $h_m F_2$ from the equilibrium state on the assumption that variations in ionospheric height caused by an $\mathbf{E} \times \mathbf{B}$ drift are negligible. Observations by the Millstone Hill radar ($\sim 51^\circ$ magnetic latitude) indicates that the uncertainties of the wind velocity incurred by ignoring the electric field effect fall within the range of uncertainties about the measurement accuracy of $h_m F_2$ and the ion drift velocity measured by the radar [28]. Igi et al. [29] estimated neutral winds from $h_m F_2$ at Kokubunji ($\sim 30^\circ$ magnetic latitude) based on the same technique used by Miller et al. [24] and the comparison with MU radar observations at Shigaraki demonstrated that wind estimate errors incurred by ignoring the $\mathbf{E} \times \mathbf{B}$ drift were not significant.

In a low-latitude region, the method of estimating neutral winds from variations in ionospheric height with $\mathbf{E} \times \mathbf{B}$ drifts ignored should fail due to the small magnetic inclination and thus a proportionate increase in the effect of $\mathbf{E} \times \mathbf{B}$ drift that induces variations in the ionospheric height. De Medeiros et al. [14] estimated neutral winds above Cachoeira Paulista ($\sim 19^\circ$ magnetic latitude) by encompassing the effect of an $\mathbf{E} \times \mathbf{B}$ drift to apply the method previously used for mid-latitude regions to low-latitude regions. The $\mathbf{E} \times \mathbf{B}$ drift used was estimated from a time derivative of $h'F$ (virtual ionospheric bottom height) scaled from ionograms collected with 15-minute intervals at Fortaleza near the magnetic equa-

tor in the same magnetic meridional plane, and mapped into the low latitude along the magnetic field line. The resultant neutral wind was in reasonable agreement with the output of the empirical neutral wind model HWM-90 [30] and measurements by a Fabry-Perot interferometer.

Bittencourt and Sahai [31] compared the values of $h_m F_2$ observed at the magnetic conjugate points in a low-latitude region that were interconnected by the same magnetic field line to estimate a neutral wind. The wind achieved with this method represents a mean transequatorial wind component at two points approximately 20° magnetic latitude apart, however winds observed at two points 3,000 km distant from each other generally vary significantly. Neutral winds are considered to be a superimposition of a component converging on the equator or diverging toward the poles and a component traversing the equator. However, the convergence/divergence component cannot be derived from observations at the magnetic conjugate points alone. Assuming that the ionospheric height in the absence of external forces can be estimated in some way and that simultaneous rises in height are observed at both points, there would be no way of telling whether such rises in height are attributable to an equatorial convergent wind or an upward $\mathbf{E} \times \mathbf{B}$ drift caused by an eastward electric field (where $\mathbf{E} \times \mathbf{B}$ drifts at the magnetic conjugate points are nearly equal).

To solve this problem and gain precise insight into ionosphere/thermosphere dynamics, we first selected three observation points along the magnetic meridional plane at 100° E, two of which were located close to the magnetic conjugate points, and the last halfway near the magnetic equator. Various ionospheric phenomena generally migrate as the sun moves west, but large-scale fluctuations not synchronized with travel of the sun are known to exist in the east-west direction, thereby contributing somewhat to ionospheric instability [32][33]. We therefore decided to install fourth and fifth ionosondes near the magnetic equator and in a low-latitude region

in Vietnam east of the 100° E north-south chain.

2 Ionosonde Observation Network

Because most of the magnetic equator susceptible to R-T plasma instability is located on the ocean as shown in Figure 1, large geographical constraints are placed on the task of putting an observation network along the magnetic meridional plane extending across the magnetic equator. Southeast Asia includes the Indochina Peninsula (north of the magnetic equator) and the Indonesian islands to the south. We had worked to build an ionospheric observation network named the Southeast Asia Low-latitude Ionospheric Network (SEALION) here. In the first place, a north-

south chain was set up at 100° E, interconnecting the ionosondes installed in the northern Thai city of Chiang Mai (the campus of Department of Agriculture, Chiang Mai University), in Chumphon, the central Malay Peninsula (the Chumphon campus of King Mongkut's Institute of Ladkrabang, Thailand), and in Kototabang, West Sumatra (at the experimental field of the Indonesian National Institute of Aeronautics and Space adjoining the Equatorial Atmosphere Radar erected by Kyoto University). Chumphon sits at 3.3° N magnetic latitude close to the magnetic equator, whereas Kototabang (0.2° S geographic latitude) and Chiang Mai (16.6° N geographic latitude) are close to magnetic conjugate points. These ionosondes are located within 1.4° longitude, and the magnetic meridional planes passing through Chiang Mai and

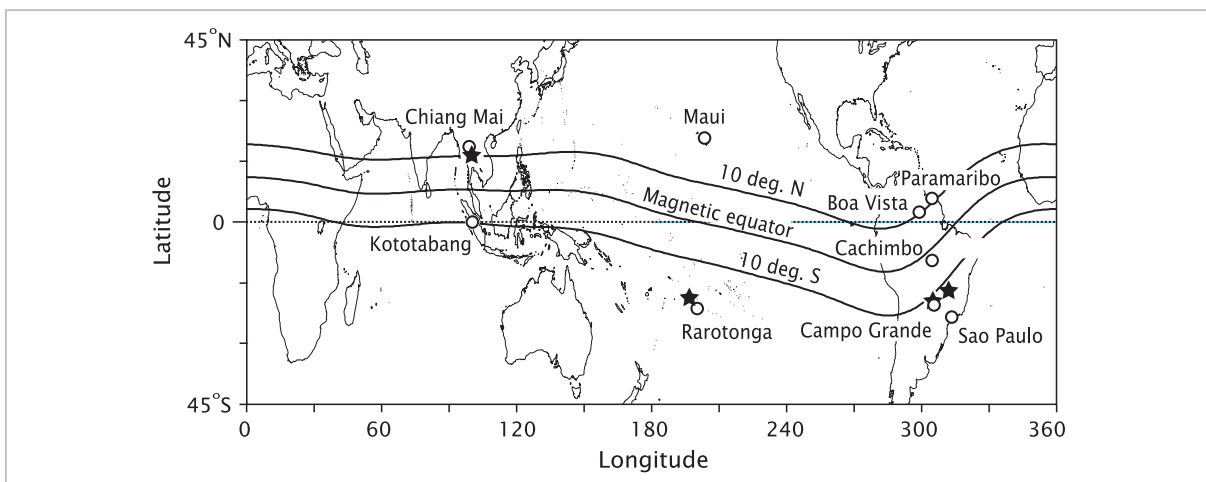


Fig. 1 Magnetic equator and 10° magnetic latitude north and south

The locations of observatories (circles) where conjugate observations have thus far been conducted are indicated, along with their magnetic conjugate points (stars) for some stations. The pairs of Paramaribo–Sao Paulo and of Maui–Rarotonga were discussed by Bittencourt and Sahai [31]; the Boa Vista–Cachimbo–Campo Grande chain was operated in the COPEX campaign [34][35].

Table 1 Location of SEALION Ionosonde

Station	Geographical coordinates		Mag. Lat	Conjugate point	
	Lon	Lat		Lon	Lat
Chiang Mai	98.9° E	18.8° N	13.0° N	99.2° E	2.3° S
Chumphon	99.4° E	10.7° N	3.3° N	99.4° E	5.6° N
Kototabang	100.3° E	0.2° S	10.0° S	100.1° E	16.6° N
Phu Thuy	106.0° E	21.0° N	15.7° N		
Bac Lieu	105.7° E	9.3° N	1.7° N		

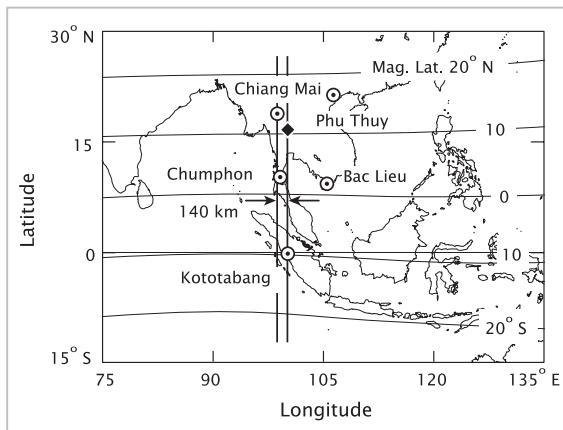


Fig.2 Ionosonde locations in the South-east Asian Ionospheric Observation Network (SEALION)

A closed diamond marks the magnetic conjugate point of Kototabang.

Kototabang are deviated only 140 km in the east-west direction. The fourth and fifth ionosondes are located in the southern Vietnamese city of Bac Lieu and the northern city of Phu Thuy, respectively (both on the premises of observatories run by the Hanoi Institute of Geophysics). The distance between Bac Lieu and Chumphon entails a longitudinal distance of 740 km at the F-region height. Figure 2 and Table 1 summarize these positional relationships, along with the relevant parameters.

Because the ionosondes installed at these remote locations must basically be run unattended, FM-CW (frequency-modulated continuous wave) ionosondes operating under low power has been newly developed. Details of this FM-CW ionosonde can be found in another paper in this special issue [36].

3 Preliminary Examination of Ionospheric Height Variations

In general, discussions of ionospheric height entail the height at which the electron density maximizes in the F-region [3][24][26][31]. One method for determining the maximum electron density height from ionosonde observations is scaling traces across the entire frequency range and performing iterative calculations

based on those traces [37]. Another method is converting the maximum electron density height from the transmission parameter $M(3000)F_2$ [38][39]. In both methods, scaling traces across the entire frequency range or scaling accurately in the vicinity of the critical frequency is a laborious task. Apparent height $h'F$ of echo trace from the F-region is used as an alternative indicator of ionospheric height. This eases the work of scaling traces from ionograms. As the ionospheric recombination process proceeds in the bottom part of the ionosphere after sunset, radio propagation delays there become negligible to make changes in $h'F$ a good indicator of ionospheric height changes. In this paper, we discuss the ionospheric dynamics with regard to $h'F$. However, care is needed in interpreting the results based on $h'F$. If the ionospheric height falls largely under the influence of external forces, the ionospheric recombination process in the bottom part of the ionosphere comes to dominate and govern $h'F$, with the result of falling ionospheric height being underestimated. If the critical frequency falls largely, particularly in pre-dawn hours, the slope of the echo trace steepens even at the lowest frequencies of the ionogram where $h'F$ is scaled. As a result, the $h'F$ comes to strongly depend on the frequency at the point scaled. Along with a constraint placed on the limited lowest operating frequency, the value of $h'F$ tends to be somewhat higher than the actual value.

While the ionospheric height is varied significantly by external forces such as drag by neutral atmospheric motion and the $\mathbf{E} \times \mathbf{B}$ drift caused by a zonal electric field, those effects can hardly be separated based on ionosonde observations alone. As a solution, we conducted model calculations under an idealized set of conditions to see how the two effects would be manifested. The model calculations attempted to solve an ion continuity equation along a magnetic field line to determine the bottomside ionospheric height [19][20]. Assumptions included a dipole-approximated magnetic field (matched geographic equator and geomagnetic equator), as well as the ver-

nal equinox and medium solar activity ($F_{10.7} = 100$). The model calculations were simplified so as to not promise more than what could be qualitatively expected from theories, but could still greatly aid in interpreting the observation results.

Figure 3 plots the results of model calculations in the presence and absence of external forces in regard to the ionospheric height at which the electron density equaled $7.75 \times 10^{10} \text{ m}^{-3}$ at 20:00; this electron density corresponds to the frequency of 2.5 MHz at which $h'F$ was scaled. The first run only included photochemical reaction and diffusion along the magnetic field lines in the absence of external forces other than gravity, which is plotted by the dotted line in the individual panels of Fig. 3 to provide a reference of comparison with the case involving the presence of external forces. A slight rise in ionospheric height is observed on the magnetic equator, but this is not an act of kinetics. Diffusion of plasma from above is restricted on the mag-

netic equator and shorter magnetic flux tubes would cause the electron density to fall rapidly after sunset upon recombination, while at low latitudes, diffusion of plasma along the field line from higher altitudes works to compensate for ionospheric extinction at the bottom.

In the next run, an upward $\mathbf{E} \times \mathbf{B}$ drift was applied and the result is shown by the thick solid line in Fig. 3a. The electric field corresponding to an $\mathbf{E} \times \mathbf{B}$ drift velocity of 30 ms^{-1} on the magnetic equator was applied at 19:00 and lasted one hour. The ionospheric height was lifted by 102 km on the magnetic equator, which was nearly equal to the upward drift of the magnetic flux tube ($30 \text{ ms}^{-1} \times 3600 \text{ s} = 108 \text{ km}$). In the low-latitude region at 10° magnetic latitude, the lift was only 38 km due to an increased downward plasma diffusion along the magnetic field lines from a higher height on the magnetic equator (fountain effect). The third run examined the effect of a transequatorial wind. The thick solid line in Fig. 3b shows the ionospheric height changes one hour after the application of a uniform northward wind of 100 ms^{-1} at 19:00 with regard to both height and latitude. The ionospheric height rose 60 km at 10° S magnetic latitude upwind, and fell 43 km at 10° N magnetic latitude downwind. The difference between the rise and fall in absolute values is associated with the effect of recombination caused by the downwind lowering of ionospheric height to suppress an apparent decline in height. A rise of about 10 km is also observed on the magnetic equator as a consequence of plasma having been blown away by winds [19]. What is more noteworthy, the ionospheric height at 10° S magnetic latitude upwind is higher than the magnetic equator. Figure 3c shows the effect of neutral winds converging on the equator. In this run, we applied a 30 ms^{-1} wind blowing toward the equator at the points of 10° magnetic latitude north and south, with winds linearly slowed down on the equatorial side to a velocity of 0 on the magnetic equator, for one hour starting at 19:00. As plasma is carried upward along the magnetic field lines in a low-latitude

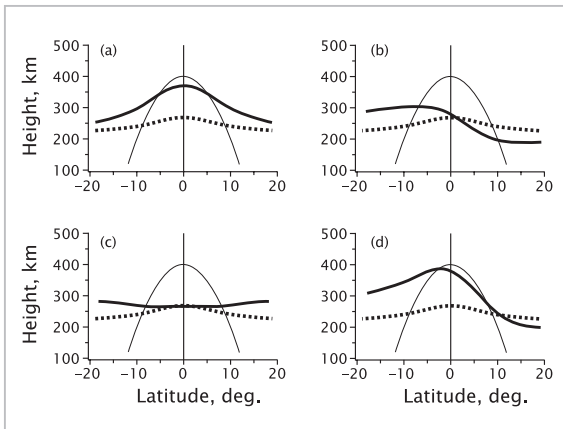


Fig.3 Model calculations of latitude changes in the ionospheric bottom height

The dotted line in each panel denotes ionospheric height, assuming the absence of external forces other than gravity. The thin line marks the magnetic field line passing 400 km above the equator. The thick line represents the (a) effect of the $\mathbf{E} \times \mathbf{B}$ drift, (b) effect of the transequatorial wind, (c) effect of a wind converging on the equator, and (d) combined effects of the $\mathbf{E} \times \mathbf{B}$ drift and transequatorial wind.

region, the ionospheric height apart from the equator becomes higher than the magnetic equator. In the last run, an $\mathbf{E} \times \mathbf{B}$ drift and a transequatorial wind were applied simultaneously and the result is shown by the thick solid line in Fig. 3d. We note that the plot is a superimposition of results given in Figs. 3a and 3b. What is important here is that an ionospheric height difference of about 100 km found between 10° magnetic latitude north and south is practically equal to the value (60 + 43 km) observed in the absence of an electric field (Fig. 3b). This finding suggests that north-south ionospheric height differences produced by transequatorial winds do not largely depend on the magnitude of the $\mathbf{E} \times \mathbf{B}$ drift velocity.

All variations in ionospheric height produced under the influence of external forces as previously described had been achieved during a one-hour period from 19:00 to 20:00. The fact that the ionospheric height resulting from external forces essentially has a cumulative effect and external forces are generally a function of time deserves notice in launching comparative studies with observation data. Figure 4 examines how soon ionospheric height changes occur. In this calculation, the changes in ionospheric height were produced by reversing the wind direction from 50 ms^{-1} northward transequatorial wind to the south-

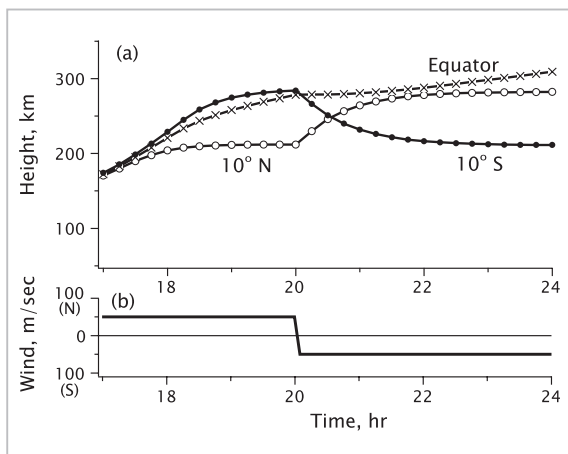


Fig.4 Response of the ionospheric height to the directional reversal of transequatorial wind shown in the lower panel

ward wind with the same strength at 20:00. Evidently, the north-south differences in ionospheric height reversed in 30 min and approached a steady state in approximately one hour.

4 Initial Results

Ionosphere/thermosphere system not only varies significantly from season to season but also involves marked day-to-day variations (weather) that origins are not always clear. We therefore decided to survey climatological views regarding particular seasons. The SEALION north-south chain yielded its first complete data set at the end of 2004. Figure 5 plots $h'F$ as scaled from ionograms taken at Chiang Mai, Chumphon, and Kototabang at 2.5 MHz with 15 min intervals at nighttime

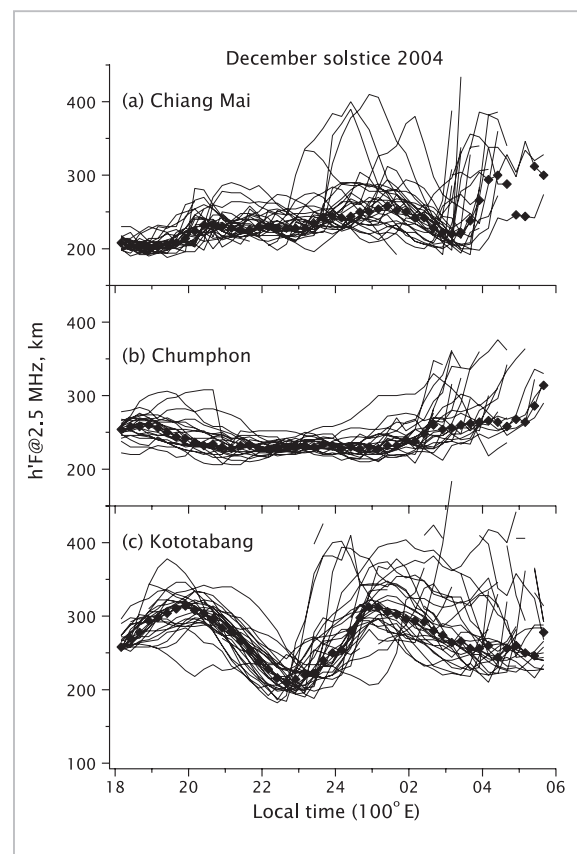


Fig.5 Nightly ionospheric height variations from December 7, 2004 to January 5, 2005 (thin continuous lines) and their medians (filled diamonds)

Apparent heights were scaled at 2.5 MHz.

from December 7, 2004 to January 5, 2005 (one month centered the December solstice). Each thin continuous line denotes a day-to-day value, whereas filled diamond denotes median values of $h'F$. Decreases in the number of data points at 04:00 LT (100° E mean time) and later reflect the critical frequency that neared or fell below 2.5 MHz. The ionospheric heights at Chiang Mai and Kototabang in the low-latitude region posted larger day-to-day variations after 23:00 LT, but such variations were small at Chumphon. This suggests that ionospheric height variations in a low-latitude region are more due to a neutral wind than an east-west electric field. Conversely, some day-to-day variations observed at Chumphon around 20:00 LT (as opposed to from 22:00 to 23:00 LT) were possibly due to variability in the zonal electric field.

Next, let us examine the distinctive behavior with regard to medians. Because ionospheric height variations at Chumphon (located near the magnetic equator) are primarily governed by the $\mathbf{E} \times \mathbf{B}$ drift, the height variations may be viewed as a measure of electric field strength. While a higher ionospheric height is reached at Kototabang than at Chumphon around 20:00 LT, this can hardly be ascribed to the $\mathbf{E} \times \mathbf{B}$ drift. Chiang Mai posted a lower ionospheric height than Chumphon and Kototabang during an earlier time period. These height behaviors in low latitude regions are ascribed to the action of a northward transequatorial wind as modeled in Fig. 3b. For more quantitative discussion, several problems are encountered. Because the solar zenith angle differs between Kototabang and Chiang Mai in the winter as both locations are separated in latitude, the neutral atmospheric composition and thermospheric temperature are also considered to vary significantly between the two observation points. Moreover, Chiang Mai and Kototabang are not exactly magnetic conjugate points, and Chiang Mai is slightly higher in magnetic latitude than Kototabang. As can be seen from the arch-like magnetic field line shown in Fig. 3a, Chiang Mai essentially tends to show a lower ionos-

pheric height than Kototabang. Model calculations were therefore conducted to determine the ionospheric height by assuming the absence of neutral winds to give a reference for the wind effect on the height. Model calculations similar to those described earlier were employed, except that the seasons were adjusted to 356 days of the year (December solstice), and a displacement of 8.2° between the magnetic latitude and the geographic latitude was used to approximate actual values. The model calculations began by adjusting the $\mathbf{E} \times \mathbf{B}$ drift velocity given to the model for reproducing the ionospheric height at Chumphon in the absence of neutral winds, in order to estimate the electric field strength. Next, electron density distribution in the magnetic meridional plane was calculated under the condition of the $\mathbf{E} \times \mathbf{B}$ drift determined, and the ionospheric height corresponding to an electron density of $7.75 \times 10^{10} \text{ ms}^{-3}$ was taken as a reference at Chiang Mai and Kototabang, respectively. Figure 6a plots the differences between the modeled reference height and the observations. Just after sunset, the observed ionospheric height at Kototabang is higher than the reference height, while that at Chiang Mai is lower than the reference height. The transequatorial wind blowing from south (summer hemisphere) to north (winter hemisphere) has a pronounced effect. With the lapse of time, the ionospheric height at Kototabang rises further, but nears the reference height at Chiang Mai. At 20:00 LT, the ionospheric height at Chiang Mai also comes to exceed the reference height. Two conditions are generally considered to account for the rises in ionospheric height at both magnetic conjugate points. One is the rising ionospheric height at all latitudes in the magnetic meridional plane resulting from an $\mathbf{E} \times \mathbf{B}$ drift. The other is the act of neutral winds converging toward the equator. Since the effect of an $\mathbf{E} \times \mathbf{B}$ drift was already considered when determining the reference height, we may conclude that the convergent wind component gradually intensified with the strength of the transequatorial wind component essentially being

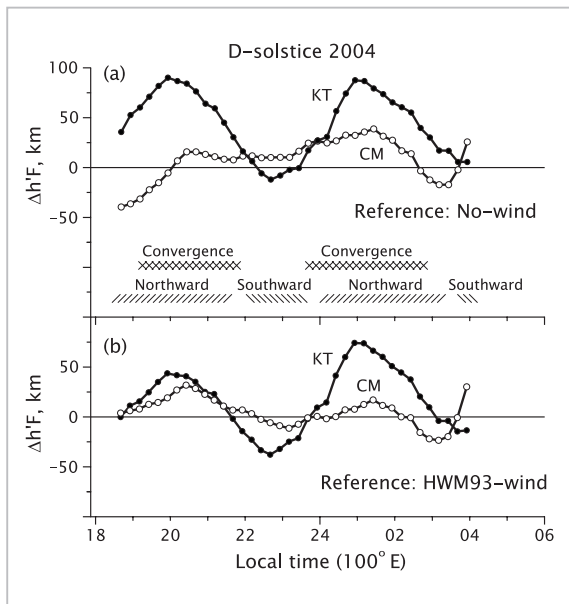


Fig.6 Differences between ionospheric reference height determined by model calculations and observations

- (a) Reference height without the influence of winds
- (b) Reference height given winds by the HWM93 model

unchanged just after sunset as shown in Fig. 6a. After 20:00 LT, the ionospheric height at Kototabang nears the reference height, but that at Chiang Mai remains somewhat above the reference height. This means that the transequatorial wind component has weakened, while the convergent wind component remains in force. At 22:00 LT, the curves at Chiang Mai and Kototabang cross each other, with the transequatorial wind reversing direction, and later reversing again at 00:00 LT. The convergent wind ceases once at 22:30 LT, and then regains strength at around 01:00 LT.

As for neutral winds, global empirical model HWM93 [40] was forged based on limited data and has often been cited for comparison with observations. A further run of model calculations was conducted for comparison with that empirical model. This time, a neutral wind as defined by HWM93 was incorporated to recalculate the $\mathbf{E} \times \mathbf{B}$ drift velocity from $h'F$ variations at Chumphon. The ionospheric reference heights at the latitudes of Kototabang

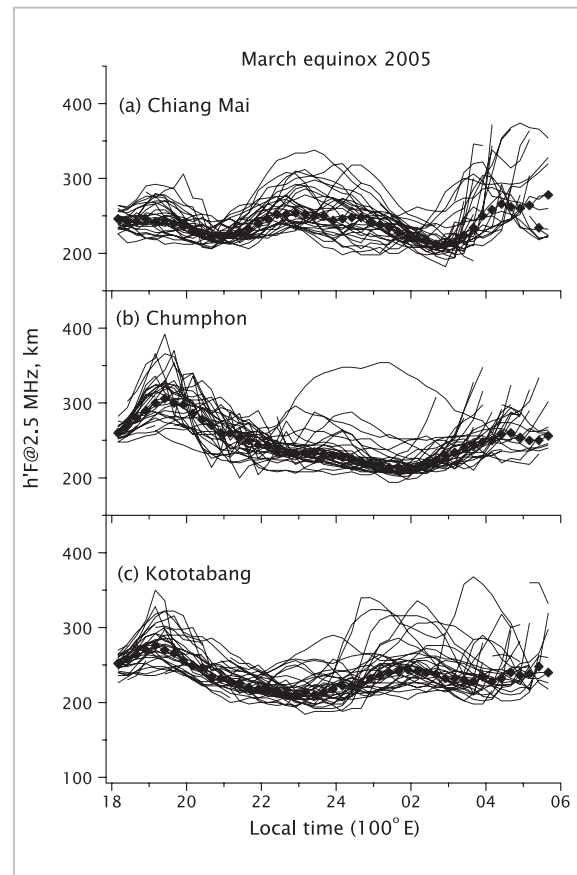


Fig.7 Same as Fig. 5 but for the period from March 5 to April 5, 2005

and Chiang Mai were established from the model calculations conducted with the resultant electric field drift and the HWM93 wind velocity field. Figure 6b shows the comparison between the modeled reference height and the observations. If the HWM93 wind velocity field is accurate, the ionospheric height variations observed by the SEALION chain should have been correctly reproduced, giving the appearance of a virtually zero line. Actually, the HWM93 calculations and observations are found in good agreement around 19:00 LT, and the difference was reduced by half at Kototabang around 20:00 LT. However, major discrepancies were noted. The peak at Kototabang after midnight remained essentially unchanged even with HWM93 enabled. What is noteworthy throughout the nighttime is that the magnitude of discrepancy varied at intervals of five to six hours at both Chiang Mai and Kototabang. The HWM93 empirical

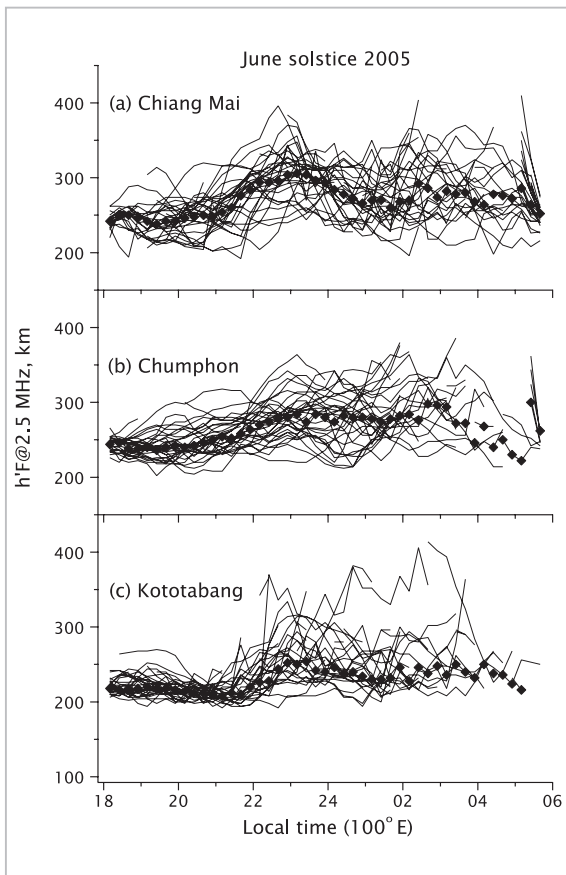


Fig.8 Same as Fig. 5 but for the period from June 5 to July 7, 2005

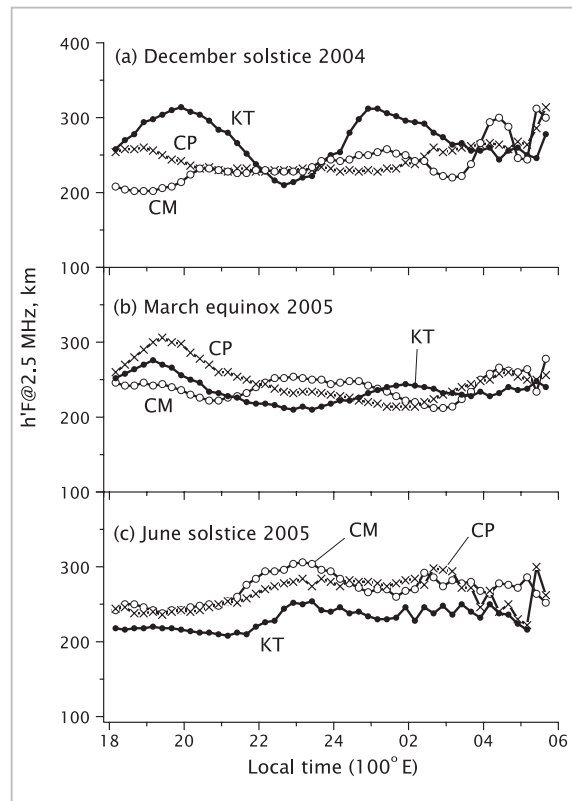


Fig.9 Median of ionospheric height by season

CM denotes Chiang Mai, CP denotes Chumphon, and KT denotes Kototabang.

model does not include variable components shorter than eight hours (terdiurnal). But such comparisons suggest that higher order variable components have a non-negligible amplitude.

Neutral winds vary significantly from season to season as the sub-solar point changes latitude. Figures 7 and 8 plot monthly ionospheric height variations at the three ionosonde locations centering on the March equinox (from March 5 to April 5, 2005), and those centering on the June solstice (from June 5 to July 7, 2005), respectively. As in Fig. 5, each thin continuous line denotes a day-to-day value, whereas filled diamond denotes a median. Figure 9 summarizes the medians shown in Figs. 5, 7, and 8 for comparing seasonal characteristics. The ionospheric height at Chumphon (on the magnetic equator) at around 19:30 LT in March (Fig. 9b) appeared higher than at lower-latitude Chiang Mai and Kototabang, with pronounced signature of

prereversal enhancement of the zonal electric field. The intensification of prereversal enhancement at both the March and September equinoxes agrees with a general tendency in electric field variations [41]. Ionospheric height differences between Chiang Mai and Kototabang are relatively smaller during these periods compared with other seasons, but the signs thereof alternate at about 6 hr intervals. The alternation of the sign is in common with the characteristics in December shown in Fig. 6, and corresponds to north-south oscillation of the transequatorial wind. A look at June (Fig. 9c) shows that Chiang Mai has always recorded a higher ionospheric height than Kototabang, indicating that a southward wind dominates during the nighttime due to the sun's location over the northern hemisphere. Characteristic differences that are not reproducible by simply reversing north and south are noted between December and June.

The displacement of the magnetic equator north of the geographic equator may have disrupted the north and south symmetry and that of summer and winter, thus adding to the complexities of the seasonal characteristics.

5 Summary

The pronounced effects of thermospheric neutral winds and a zonal electric field exerted upon the equatorial and low-latitude ionosphere, combined with a tight north-south coupling, result in characteristics not found in other latitudes. We have built five ionosonde stations in Southeast Asia in order to launch an ionosphere observation program for gaining detailed insight into the equatorial ionospheric phenomena including plasma bubbles (equatorial spread-F). The ionospheric height was derived among these points from initial data collected at three locations in the north-south chain at 100° E longitude, and then subjected to statistical analyses. The effects of the electric field and a neutral wind were separated from each other based on ionospheric height comparisons, and identified seasonal characteristics of the ionosphere/thermosphere system. Winds were found to have characteristics significantly different from those of empirical model HWM93, including variations at about 6 hr intervals. The behavior of neutral winds is so important in terms of plasma instability that further probes into certain issues, such as its bearing on the formation of plasma bubbles, will be detailed in other

papers [42][43] in this special issue.

Neutral winds converging on the equator identified from SEALION were found to have a tight connection with the phenomenon of nighttime temperature rises known as “MTM” (midnight temperature maximum) in the low-latitude thermosphere [44], which was not included in this article. Although the relation between MTM and the formation of plasma bubbles remains unknown, the strong association of MTM with lower-atmospheric motion has been suggested. Research on the issue of the middle and lower atmosphere coupling with the ionosphere/thermosphere as reported in **3–4** in this special issue has just begun, and could provide clues to solving ionospheric challenges. This may suggest an important direction in the evolving course of our ionospheric space weather studies.

Acknowledgements

The SEALION Project has been pursued jointly with research institutes and universities in Thailand, Indonesia, and Vietnam. We wish to thank King Mongkut’s Institute of Technology Ladkrabang and Chiang Mai University both in Thailand, the Indonesian National Institute of Aeronautics and Space, the Hanoi Institute of Geophysics, Vietnam, and Kyoto University’s Research Institute for Sustainable Humanosphere, which constructed and operates a radar facility in Sumatra, Indonesia, for their significant support and cooperation.

References

- 1 S. Chapman, “The absorption and dissociative or ionizing effect of monochromatic radiation in an atmosphere on a rotating earth,” *Proc. Phys. Soc.*, Vol. 43, pp. 26–45, 1931.
- 2 T. Yonezawa, “Theory of formation of the ionosphere,” *Space Sci. Rev.*, Vol. 5, pp. 3–56, 1966.
- 3 H. Rishbeth, S. Ganguly, and J. C. G. Walker, “Field-aligned and field-perpendicular velocities in the ionospheric F2-layer,” *J. Atmos. Terr. Phys.*, Vol. 40, pp. 767–784, 1978.
- 4 D. F. Strobel and M. B. McElroy, “The F2-layer at middle latitudes,” *Planet. Space Sci.*, Vol. 18, pp. 1181–1202, 1970.
- 5 T. Tanaka and K. Hirao, “Effects of an electric field on the dynamical behavior of the ionospheres and its application to the storm time disturbance of the F-layer,” *J. Atmos. Terr. Phys.*, Vol. 35, pp. 1443–1452, 1973.

- 6 W. B. Hanson and R. J. Moffett, "Ionization transport effects in the equatorial F region," *J. Geophys. Res.*, Vol. 71, pp. 5559–5572, 1966.
- 7 D. N. Anderson, "A theoretical study of the ionospheric F region equatorial anomaly -2. Results in the American and Asian sectors," *Planet. Space Sci.*, Vol. 21, pp. 421–442, 1973.
- 8 S. Namba and K. Maeda, "Radio wave propagation," Corona Publishing, Tokyo, p. 86, 1939.
- 9 H. Rishbeth, "The equatorial F-layer: Progress and puzzles," *Ann. Geophys.*, Vol. 18, pp. 730–739, 2000.
- 10 R. P. Sharma and E. J. Hewens, "A study of the equatorial anomaly at American longitudes during sunspot minimum," *J. Atmos. Terr. Phys.*, Vol. 38, pp. 475–484, 1976.
- 11 T. Maruyama and N. Matuura, "Longitudinal variability of annual changes in activity of equatorial spread F and plasma bubbles," *J. Geophys. Res.*, Vol. 89, No. A12, pp. 10903–10912, 1984.
- 12 G. O. Walker and H. F. Chan, "Computer simulations of the seasonal variations of the ionospheric equatorial anomaly in East Asia under solar minimum conditions," *J. Atmos. Terr. Phys.*, Vol. 51, pp. 953–974, 1989.
- 13 J. E. Titheridge, "The calculation of neutral winds from ionospheric data," *J. Atmos. Terr. Phys.*, Vol. 57, pp. 1015–1036, 1995.
- 14 R. T. de Medeiros, M. A. Abdu, and I. S. Batista, "Thermospheric meridional wind at low latitude from measurements of F layer peak height," *J. Geophys. Res.*, Vol. 102, No. A7, pp. 14531–14540, 1997.
- 15 N. Matuura, "Electric fields deduced from the thermospheric model," *J. Geophys. Res.*, Vol. 79, pp. 4679–4689, 1974.
- 16 R. A. Heelis, P. C. Kendall, R. J. Moffett, D. W. Windle, and H. Rishbeth, "Electrical coupling of the E- and F-regions and its effect on F-region drifts and winds," *Planet. Space Sci.*, Vol. 22, pp. 743–756, 1974.
- 17 D. T. Farley, E. Bonelli, B. G. Fejer, and M. F. Larsen, "The prereversal enhancement of the zonal electric field in the equatorial ionosphere," *J. Geophys. Res.*, Vol. 91, No. A12, pp. 13723–13728, 1986.
- 18 J. V. Eccles, "Modeling investigation of the evening prereversal enhancement of the zonal electric field in the equatorial ionosphere," *J. Geophys. Res.*, Vol. 103, No. A11, pp. 26709–26719, 1998.
- 19 T. Maruyama, "Modeling study of equatorial ionospheric height and spread F occurrence," *J. Geophys. Res.*, Vol. 101, No. A3, pp. 5157–5163, 1996.
- 20 T. Maruyama, "A diagnostic model for equatorial spread F, 1. Model description and application to electric field and neutral wind effects," *J. Geophys. Res.*, Vol. 93, No. A12, pp. 14611–14622, 1988.
- 21 M. Mendillo, J. Baumgardner, X. Pi, P. J. Sultan, and R. Tsunoda, "Onset conditions for equatorial spread F," *J. Geophys. Res.*, Vol. 97, No. A9, pp. 13865–13876, 1992.
- 22 S. Saito and T. Maruyama, "Ionospheric height variations observed by ionosondes along magnetic meridian and plasma bubble onsets," *Ann. Geophys.*, Vol. 24, pp. 2991–2996, 2006.
- 23 M. J. Buonsanto, "Seasonal variations of day-time ionization flows inferred from a comparison of calculated and observed N_mF_2 ," *J. Atmos. Terr. Phys.*, Vol. 48, pp. 365–373, 1986.
- 24 K. L. Miller, D. G. Torr, and P. G. Richards, "Meridional winds in the thermosphere derived from measurement of F2 layer height," *J. Geophys. Res.*, Vol. 91, No. A4, pp. 4531–4535, 1986.
- 25 K. L. Miller, M. Lemon, and P. G. Richards, "A meridional wind climatology from a fast model for the derivation of meridional winds from the height of the ionospheric F2 region," *J. Atmos. Solar-Terr. Phys.*, Vol. 59, pp. 1805–1822, 1997.
- 26 P. G. Richards, "An improved algorithm for determining neutral winds from the height of the F2 peak electron density," *J. Geophys. Res.*, Vol. 96, No. A10, pp. 17839–17846, 1991.

- 27 L. Liu, X. Luan, W. Wan, B. Ning, and J. Lei, "A new approach to the derivation of dynamic information from ionosonde measurements," *Ann. Geophys.*, Vol. 21, pp. 2185–2191, 2003.
- 28 K. L. Miller, J. E. Salah, and D. G. Torr, "The effect of electric fields on measurements of meridional neutral winds in the thermosphere," *Ann. Geophys.*, Vol. 5A, pp. 337–342, 1987.
- 29 S. Igi, T. Ogawa, W. L. Oliver, and S. Fukao, "Thermospheric winds over Japan: Comparison of ionosonde and radar measurements," *J. Geophys. Res.*, Vol. 100, No. A11, pp. 21323–21326, 1995.
- 30 A. E. Hedin, M. A. Biondi, R. G. Burnside, G. Hernandez, R. M. Johnson, T. L. Killeen, C. Mazaudier, J. W. Meriwether, J. E. Salah, R. J. Sica, R. W. Smith, N. W. Spencer, V. B. Wickwar, and T. S. Virdi, "Revised global model of thermosphere winds using satellite and ground-based observations," *J. Geophys. Res.*, Vol. 96, No. A5, pp. 7657–7688, 1991.
- 31 J. A. Bittencourt and Y. Sahai, "F-region neutral winds from ionosonde measurements of $h_m F_2$ at low latitude magnetic conjugate regions," *J. Atmos. Terr. Phys.*, Vol. 40, pp. 669–676, 1978.
- 32 M. C. Kelley, M. F. Larsen, C. La Hoz, and J. P. McClure, "Gravity wave initiation of equatorial spread F: A case study," *J. Geophys. Res.*, Vol. 86, No. A11, pp. 9087–9100, 1981.
- 33 R. T. Tsunoda, "On the enigma of day-to-day variability in equatorial spread F," *Geophys. Res. Lett.*, Vol. 32, L08103, doi:10.1029/2005GL022512, 2005.
- 34 B. W. Reinisch, M. Abdu, I. Batista, G. S. Sales, G. Khmyrov, T. A. Bullett, J. Chau, and V. Rios, "Multi-station digisonde observations of equatorial spread F in South America," *Ann. Geophys.*, Vol. 22, pp. 3145–3153, 2004.
- 35 M. A. Abdu, I. S. Batista, B. W. Reinisch, and A. J. Carrasco, "Equatorial F-layer heights, evening prereversal electric field, and night E-layer density in the American sector: IRI validation with observations," *Adv. Space Res.*, Vol. 34, pp. 1953–1965, 2004.
- 36 K. Nozaki, "FMCW ionosonde for the SEALION Project," Special issue of this NICT Journal, 3–2–5, 2009.
- 37 J. E. Titheridge, "The real height analysis of ionograms: A generalized formulation," *Radio Sci.*, Vol. 23, pp. 831–849, 1988.
- 38 T. Shimazaki, "World-wide daily variations in the height of the maximum electron density of the ionospheric F2 layer," *J. Radio Res. Labs.*, Vol. 2, pp. 85–97, 1955.
- 39 F. T. Berkey and G. H. Stonehocker, "A comparison of the height of the maximum electron density of the F2-layer from real height analysis and estimates based on $M(3000)F_2$," *J. Atmos. Terr. Phys.*, Vol. 51, pp. 873–877, 1989.
- 40 A. E. Hedin, E. L. Fleming, A. H. Manson, F. J. Schmidlin, S. K. Avery, R. R. Clark, S. J. Franke, G. J. Fraser, T. Tsuda, F. Vial, and R. A. Vincent, "Empirical wind model for the upper, middle and lower atmosphere," *J. Atmos. Solar-Terr. Phys.*, Vol. 58, pp. 1421–1447, 1996.
- 41 B. G. Fejer, E. R. de Paula, R. A. Heelis, and W. B. Hanson, "Global equatorial ionospheric vertical plasma drifts measured by the AE-E satellite," *J. Geophys. Res.*, Vol. 100, No. A4, pp. 5769–5776, 1995.
- 42 S. Saito and T. Maruyama, "Effects of transequatorial thermospheric wind on plasma bubble occurrences," Special issue of this NICT Journal, 3–2–2, 2009.
- 43 S. Saito and T. Maruyama, "Large-scale zonal structure of the equatorial ionosphere and equatorial spread F occurrence," Special issue of this NICT Journal, 3–2–3, 2009.
- 44 T. Maruyama, S. Saito, M. Kawamura, and K. Nozaki, "Thermospheric meridional winds as deduced from ionosonde chain at low and equatorial latitudes and their connection with midnight temperature maximum," *J. Geophys. Res.*, Vol. 113, A09316, doi:10.1029/2008JA013031, 2008.

MARUYAMA Takashi, Ph.D. (Eng.)
Executive Researcher
Upper Atmospheric Physics



SAITO Susumu, Ph.D.
*Senior Researcher, Communication,
Navigation, and Surveillance
Department, Electronic Navigation
Research Institute*
Aeronomy, Satellite Navigation

KAWAMURA Masabumi
*Former : Technical Expert, Space
Environment Group, Applied
Electromagnetic Research Center*
Computer Network



NOZAKI Kenro
Telecom Engineering Center
Space Environment

UEMOTO Jyunpei, Ph.D.
*Expert Researcher, Space Environment
Group, Applied Electromagnetic
Research Center*
Aeronomy



TSUGAWA Takuya, Ph.D.
*Expert Researcher, Space Environment
Group, Applied Electromagnetic
Research Center*
Upper Atmosphere Physics



JIN Hidekatsu, Dr. Sci.
*Expert Researcher, Space Environment
Group, Applied Electromagnetic
Research Center*
Upper Atmospheric Physics

ISHII Mamoru, Dr. Sci.
*Director, Project Promotion Office,
Applied Electromagnetic Research
Center*
Upper Atmospheric Physics



KUBOTA Minoru, Ph.D.
*Senior Researcher, Space Environment
Group, Applied Electromagnetic
Research Center*
Aeronomy